Solid State H-2 NMR Analysis of Furanose Ring Dynamics in DNA Containing Uracil

ARTICLE *in* THE JOURNAL OF PHYSICAL CHEMISTRY B · FEBRUARY 2010

Impact Factor: 3.3 · DOI: 10.1021/jp9091656 · Source: PubMed

5 AUTHORS, INCLUDING:

Monica Kinde
University of Pittsburgh
10 PUBLICATIONS **15** CITATIONS
SEE PROFILE

Gerard S. Harbison
University of Nebraska at Lincoln
99 PUBLICATIONS **2,658** CITATIONS
SEE PROFILE

Published in final edited form as:
J Phys Chem B. 2010 March 11; 114(9): 3285–3293. doi:10.1021/jp9091656.

Solid State ^{2}H NMR Analysis of Furanose Ring Dynamics in DNA Containing Uracil

Monica N. Kinde-Carson[†], **Crystal Ferguson**[§], **Nathan A. Oyler**[‡], **Gerard S. Harbison**[†], and **Gary A. Meints**[*,§]

Department of Chemistry, University of Nebraska, Lincoln, Nebraska 68588, Department of Chemistry, University of Missouri–Kansas City, Kansas City, Missouri 64110, Department of Chemistry, Missouri State University, Springfield, Missouri 65897

[†]University of Nebraska.

[‡]University of Missouri-Kansas City.

[§]Missouri State University.

Abstract

DNA damage has been implicated in numerous human diseases, particularly cancer, and the aging process. Single-base lesions, such as uracil, in DNA can be cytotoxic or mutagenic and are recognized by a DNA glycosylase during the process of base excision repair. Increased dynamic properties in lesion-containing DNAs have been suggested to assist recognition and specificity. Deuterium solid-state nuclear magnetic resonance (SSNMR) has been used to directly observe local dynamics of the furanose ring within a uracil: adenine (U:A) base pair and compared to a normal thymine:adenine (T:A) base pair. Quadrupole echo lineshapes, $\langle T_{1Z} \rangle$, and $\langle T_{2e} \rangle$ relaxation data were collected, and computer modeling was performed. The results indicate that the relaxation times are identical within the experimental error, the solid lineshapes are essentially indistinguishable above the noise level, and our lineshapes are best fit with a model that does not have significant local motions. Therefore, U:A base pair furanose rings appear to have essentially identical dynamic properties as a normal T:A base pair, and the local dynamics of the furanose ring are unlikely to be the sole arbiter for uracil recognition and specificity in U:A base pairs.

I. Introduction

The integrity of DNA structure must be maintained for proper cellular function and viability of the genome. Numerous processes create single-base lesions and mismatches in DNA, including alkylation, oxidation, deamination, and incorporation of improper nucleotides. An estimated 10^4–10^6 DNA damage events occur per cell per day in humans.[1] One particularly common error is the presence of uracil (U) in DNA that arises either due to misincorporation of dUMP/dUTP or deamination of cytosine, creating a cytosine to thymine (C → T) transition mutation.[2] Deamination produces the mutagenic U:G base pairs, whereas improper dUMP/dUTP incorporation produces potentially cytotoxic U:A base pairs.[2]

Removal of uracil involves the base excision repair (BER) pathway, a primary repair mechanism of single-base lesions in DNA.[1,3-8] The initial steps of BER, performed in this case by uracil DNA glycosylase (UNG), consist of recognition of the damage site, formation of a

[*]Corresponding author. Phone: 417 836 6291. Fax: 417 836 5507. garymeints@missouristate.edu. .

specific complex, and removal of the lesion. During the removal step, the lesion-containing nucleotide is rotated out of the DNA helix and stabilized in the binding pocket of the glycosylase in a process known as nucleotide flipping or base flipping. Nucleotide flipping is a common motif in DNA–protein interactions,[9] used by glycosylases, methyltransferases, glucosyltransferases, and photolyases. In particular, UNG has been shown to flip its target site,[10] and deoxyuridine is a substrate in both U:G and U:A base pairing contexts.[2]

Many details of BER have been elucidated, but the exact mechanism of lesion recognition in the presence of a vast excess of normal DNA bases remains elusive. The lesions are often similar structurally to normal DNA bases, suggesting that direct recognition of the damaged base itself may not play a primary or singular role. Indeed, structural studies of free DNA containing single-base lesions have shown varying degrees of deviation from canonical B-form DNA.[11] Few structural studies comparing undamaged dsDNA to uracil-containing dsDNA have been performed. Delort and co-workers found a modest change in the *N*-glycosidic bond torsion angle as the only alteration due to the presence of a uracil replacing a thymine.[12] Several NMR studies with uracil-containing hairpins have been performed,[11,13] revealing more substantial local structural changes. Raman spectroscopy has shown that uracil-containing dsDNA and normal dsDNA are essentially indistinguishable.[14] These data seem to suggest that a static structural component may not play a significant role in the recognition of uracil by UNG, given the tremendous specificity that UNG has for its substrate. However, other properties in uracil-containing DNA have been shown to differ; in particular, thermodynamic parameters vary significantly in DNA containing uracil in various base-pairing contexts.[15]

It has been proposed that a dynamic component or flexibility of the lesion nucleotide plays a significant role in the biomolecular recognition process of DNA lesions,[16] and recognition of the local flexibility of the lesion site is likely the first step to identification by the glycosylase.[17] Solution NMR techniques have been used to probe base-pair opening dynamics from imino exchange.[18,19] Wild-type UNG and a series of mutants with single-residue active site mutations were expressed, and their effects on the imino exchange rate was determined. These studies concluded that mutant UNG increases the lifetime of open T:A base pairs, accelerates the imino exchange of the thymine, and suggests that UNG takes advantage of increased base pair opening dynamics in T:A and U:A base pairs. Additionally, DNAs containing artificially constrained sugars have been shown to change UNG activity due to nonideal rigid sugar conformation.[20] A dynamic sugar ring alleviates resistance to conformational rearrangement, facilitating the necessary structure for catalysis.

Deuterium (^{2}H) solid-state NMR (SSNMR) has been used to directly examine the dynamic properties in the furanose ring of DNA containing uracil (U:A base pair), as compared to a normal (T:A) base pair (Figure 1). Previous ^{2}H SSNMR investigations have studied the sequence-dependent dynamics within the binding site of the *Hha*I methyltransferase,[21-25] an enzyme which also uses nucleotide flipping during its methylation process.[26] These SSNMR results indicate the furanose ring and backbone methylene groups of the target deoxycytidine residue have the greatest dynamic properties (ring puckering amplitude, rate, and lowest energetic barriers to conformational rearrangement), and it was suggested that these properties contribute to either recognition of the target dC or nucleotide flipping, or both.

DNA sequences containing [2″-^{2}H] deuterated derivatives of thymidine and deoxyuridine (Figure 1B) were synthesized and incorporated into 12-bp oligonucleotides (Figure 1A). Each solid DNA sample was hydrated to 10 ± 1 waters per nucleotide. Under these conditions, local hydration is substantially complete, so local dynamics are essentially solution-like; introduction of additional waters only adds to bulk hydration, facilitating global tumbling around the helical axis and negating the advantages of the SSNMR technique.

The work herein addresses the question of whether dynamic properties of the lesion-containing DNA furanose ring are the sole or primary property that facilitates recognition of uracil by UNG in U:A base pair contexts. We use deuterium SSNMR because it represents a powerful technique for directly observing dynamic properties in macromolecules. Quadrupole echo line shape, $\langle T_{1Z} \rangle$, and $\langle T_{2e} \rangle$ relaxation data were collected for both sequences in Figure 1A, and computer modeling was performed. The results indicate that the relaxation times are identical within the experimental error, the solid lineshapes are essentially indistinguishable above the noise level, and our lineshapes are best fit with a model that does not have significant local motions. Therefore, U:A base pair furanose rings appear to have dynamic properties that are essentially identical to a normal T:A base pair, and the local dynamics of the furanose ring may not play an important role for uracil recognition in U:A base pairs.

II. Experimental

Synthesis of Selectively Deuterated DNAs

[2″-H]-2′-deoxyuridine and [2″-^{2}H]-thymidine nucleosides for deuterium dynamics experiments were prepared using well-established methods.[27] Deuteration was confirmed by proton solution NMR of the labeled nucleoside monomers. Loss of integrated signal intensity of the appropriate peaks and changes in splitting patterns of coupled protons are recorded for all labeled monomers. Conversion to the 5′-*O*-(dimethoxytrityl)-3′-*O*-(2-cyanoethyl-*N*,*N*-diisopropylphosphoramidite derivatives was also performed using well-established methods.[28]

Automated DNA synthesis was outsourced to SynGen Inc. (Hayward, CA). Two × 10 μmol syntheses were performed with the labeled amidites discussed above using standard automated synthesis procedures. The following DNA 12-mer constructs were used, where the underlined residue contains the deuterium label: 5′-CGCGAAT<u>T</u>CGCG-3′ (T:A sample) and 5′-CGCGAAT<u>U</u>CGCG-3′ (U:A sample). The control sequence is the well-known Dickerson dodecamer,[29] because furanose ring motion within this sequence has been extensively studied via solid-state deuterium NMR.[30-34] These prior investigations made this sequence a particularly attractive control, and any changes to the appropriate properties due to the replacement of a thymine with a single uracil could be monitored and compared to previous work.

Twenty-two milligrams (T:A) and 42.8 mg (U:A) of DNA were weighed, salted to 10% w/w with NaCl, heated to 75 °C for 10–15 min, cooled to room temperature for 1 h for annealing, then frozen using liquid nitrogen and lyophilized. To remove residual HDO, samples were redissolved in deuterium-depleted water and then lyophilized twice. The dry sample was packed into a 4 mm sample chamber (standard NMR tube, cut to fit static solid probe) and placed in sealed hydration chambers (79% relative humidity) over saturated salt solutions containing deuterium-depleted water.[35] Water addition (W = number of waters per nucleotide) to the samples was monitored gravimetrically to a hydration level of 10 ± 1. Samples were then sealed and allowed to equilibrate an additional week before use in NMR experiments. Water introduced to salted nucleic acids progressively populates the grooves, bases, and backbone in a well-characterized fashion, beginning with the phosphates and eventually reaching limiting local hydration such that subsequent addition of water contributes primarily to the surrounding water shells.[36] At W = 10, local hydration of the nucleic acid backbone and bases is substantially complete.[36-38] Global tumbling, however, is still partially suppressed at this hydration level. The measured dynamics once hydration has reached W = 10 should thus be reflective of the local motions present in solution, whereas global motions are suppressed.

Solid-State NMR Spectroscopy

All experiments were performed on a 14 T Avance NMR spectrometer (Bruker Biospin, Billerica, MA), using a home-built, singly tuned, solid-state NMR probe. The sample coil was 4 mm in internal diameter, giving a deuterium $\pi/2$ pulse of 1.8 μs. Unless otherwise specified, the pulse delay between the two pulses in the quadrupolar echo sequence was 40 μs.

Following shifting to the echo, deuterium free-induction decays were processed with 2 kHz exponential apodization prior to Fourier transformation. $\langle T_{2e} \rangle$ relaxation times reported in this paper are obtained by varying the echo delay. After the very slowly varying HDO background signal was subtracted, weighted integrals of the spin echoes were extracted as a function of the delay between the quadrupole echo $\pi/2$ pulse and fit to a single-exponential function. The time constant of that function is simply the $\langle T_{2e} \rangle$. Spin–lattice relaxation times reported in this paper are obtained by saturation recovery; echo amplitudes, after HDO subtraction, were extracted as a function of the delay between acquisitions and fit to a single-exponential function. The time constant of that function, making the reasonable assumption that a hard pair of $\pi/2$ pulses followed by a free induction decay leaves the system saturated, is simply the $\langle T_1 \rangle$.

III. Theory

The theory of general internal molecular dynamics as probed by deuterium SSNMR is well-documented.[39,40] The fundamental theoretical relationships used to interpret the spectroscopic data describing the internal motions of DNA subunits—in particular the furanose ring—have been described.[23,34] A dynamically modulated deuterium NMR line shape is obtained via a quadrupolar echo experiment $[(\pi/2)_x - \tau - (\pi/2)_y - \tau - \text{acq})]$. The response of the deuterium spin system starting at the peak of the echo is governed by the equation of motion:

$$\frac{\mathrm{d}m(t)_{\pm}}{\mathrm{d}t} = A_{\pm} m(t)_{\pm} \tag{1}$$

where $m(t)$ is the time domain response and

$$A_{\pm} = i\omega_{\pm} + \pi \tag{2}$$

where ± labels either the transition from $m = -1$ to $m = 0$ or from $m = 0$ to $m = +1$, π is a matrix composed of site exchange rates, and $\omega_{\pm}$ is a diagonal matrix with nonzero elements that are the orientation-dependent frequencies

$$\omega_{\pm}^{i} = \pm \frac{3}{4} \frac{\mathrm{e}^2 qQ}{\hbar} \sum_{a=-2}^{+2} D_{0,a}^{(2)} \left(\Omega_i^{\mathrm{PC}} \right) D_{a,0}^{(2)} \left(\Omega^{\mathrm{CL}} \right) \tag{3}$$

where the super/subscript i denotes the ith of N structural sites. The crystal-fixed frame of the ith site is related to the principal axis system of the EFG tensor by the solid angle $\Omega_i^{\mathrm{PC}} = (0, \theta_i, \phi_i)$. Because the sample is assumed to be polycrystalline, an additional solid angle $\Omega_i^{\mathrm{CL}} = (\phi_{\mathrm{CL}}, \theta_{\mathrm{CL}}, 0)$ relates the crystal-fixed frame to the laboratory-fixed frame.

The effect of the second 90° pulse is to reverse quadrupolar precession. Therefore, if detection of the free induction decay is initiated at the top of the echo, the solution of eq 1 is

$$m_{\pm}(t) = \overrightarrow{1} \bullet \mathrm{e}^{A_{\pm}(t+\tau_2)} \bullet \mathrm{e}^{A^*_{\pm}\tau_1} \bullet \overrightarrow{m}_0 \tag{4}$$

where $A^*_{\pm} = -i\omega_{\pm} + \pi = -i\omega_{\pm} + \pi$. If the matrices T and T^* diagonalize A and A^*, respectively (i.e., $T^{-1}AT = \lambda$ and $(T^*)^{-1}A^*T^* = \lambda^*$), the time domain signal may be expanded as

$$m(t) = \overrightarrow{1} \bullet T\mathrm{e}^{\lambda(t+\tau_2)}T^{-1} \bullet T^*\mathrm{e}^{\lambda^*\tau_1}(T^*) \bullet \overrightarrow{m}_0 = \sum_{j,k,l,m,n} T_{jk}\mathrm{e}^{\lambda(t+\tau_2)}T^{-1}_{kl}T^*_{lm}\mathrm{e}^{\lambda^*_m\tau_1}(T^*)^{-1}_{mn}m_{0,n} = \sum_k b_k \mathrm{e}^{\lambda_k t} \tag{5}$$

The orientation-dependent line shape is just the Fourier transform of eq 5,

$$I(\omega, \tau_1, \tau_2, \Omega_{\mathrm{CL}}) = Re\int_{-\infty}^{+\infty} m(t)\,\mathrm{e}^{-i\omega t}\mathrm{d}t = Re\sum_k \frac{b_k}{\lambda_k - i\omega} \tag{6}$$

In a polycrystalline sample, the line shape is averaged over all orientations:

$$I(\omega, \tau_1, \tau_2) = \int_0^{2\pi}\mathrm{d}\phi_{\mathrm{CL}}\int_0^{\pi}\mathrm{d}\theta_{\mathrm{CL}}\,\sin\theta_{\mathrm{CL}}\,I(\omega, \tau_1, \tau_2, \phi_{\mathrm{CL}}, \theta_{\mathrm{CL}}) \tag{7}$$

Equation 7 is the theoretical form for the motionally modulated deuterium line shapes presented in this paper. For kinetic models involving jumps between discrete sites, eq 7 is evaluated numerically using the program MXET1,[40] which also allows calculation of line shapes modulated by motions around multiple axes. In helical DNA at hydration levels of $W = 10$ and higher, simulations include a uniform rotation around the long helical axis[41] in addition to strictly local motions of the furanose rings or other subunits, such as the backbone C5′-methylene. A second motional axis would require an additional transformation in eq 3 representing the motion around the helical axis.

$T_{2\mathrm{e}}$ relaxation is determined by plotting the decay of the signal intensity as a function of quadrupole echo delay. This value is most sensitive to slow motion, on the order of microseconds to milliseconds. For short oligonucletoides, this analysis probes the longitudinal motion about the helical axis and possible slower motions of the furanose ring, which might include pucker inversions. Powder-averaged spin–lattice relaxation is sensitive to motions on the nanosecond to microsecond time scales. For short oligonucleotides, this type of timescale will be most sensitive to differences in local motions of the appropriate subunits, which in this case is the furanose ring. Spin–lattice relaxation times reported in this paper are obtained by simple saturation recovery. The partly recovered orientation dependent line shape is, as a function of the recovery time t_{r}:

$$I(\omega, \tau_1, \tau_2, t_r, \Omega_{\mathrm{CL}}) = \left(1 - \mathrm{e}^{-t_r/T_1}\right) I(\omega, \tau_1, \tau_2, \infty, \Omega_{\mathrm{CL}}) \tag{8}$$

In eq 8, the spin–lattice relaxation time for deuterium nuclei is

$$\frac{1}{T_1} = \frac{3}{16}\left(\frac{\mathrm{e}^2qQ}{\hbar}\right)^2 \left(J_1(\omega, \theta_{\mathrm{CL}}, \varphi_{\mathrm{CL}}) + 4J_2(2\omega, \theta_{\mathrm{CL}}, \varphi_{\mathrm{CL}})\right) \tag{9}$$

where

$$J_{\mathrm{q}}(q\omega) = Re\int_{-\infty}^{+\infty} C_{\mathrm{q}}(t)\, \mathrm{e}^{i\omega t}\, \mathrm{d}t \tag{10}$$

In eq 10, $C_{\mathrm{q}}(t)$ is the autocorrelation function defined as

$$C_{\mathrm{q}}(t) = \sum_{p,p'} D_{pq}^{(2)^*}(\Omega_{\mathrm{CL}})\, D_{p'q}^{(2)}(\Omega_{\mathrm{CL}}) \left\langle D_{0p}^{(2)*}(\Omega_{\mathrm{PC}}(0))\; D_{0p'}^{(2)}(\Omega_{\mathrm{PC}}(t)) \right\rangle \tag{11}$$

where

$$\begin{aligned} &\left\langle D_{0p}^{(2)^*}(\Omega_{\mathrm{PC}}(0))\; D_{0p'}^{(2)}(\Omega_{\mathrm{PC}}(t)) \right\rangle \\ &\quad = \int \mathrm{d}\Omega_{\mathrm{PC}}(0) \int \mathrm{d}\Omega_{\mathrm{PC}}(t)\, D_{0p}^{(2)^*}(\Omega_{\mathrm{PC}}(0)) \\ &\quad \times D_{0p'}^{(2)}(\Omega_{\mathrm{PC}}(t))\; P(\Omega_{\mathrm{PC}}(t) \\ &\quad , t|(\Omega_{\mathrm{PC}}(0))\; W(\Omega_{\mathrm{PC}}(0)) \end{aligned} \tag{12}$$

$P(\omega_{\mathrm{PC}}(t), t|\omega_{\mathrm{PC}}(0))$ is the conditional probability of the C–D vector reorienting to $\omega_{\mathrm{PC}}(t)$ from $\omega_{\mathrm{PC}}(0)$ at a time t earlier, and $W(\omega_{\mathrm{PC}}(0))$ is the a priori probability of the bond being oriented at $\omega_{\mathrm{PC}}(0)$.

Models of DNA Helix Motion

In addition to simulating the motion of the particular sugar rings in question, it was necessary to resolve other types of motion that were present in the sample. For hydration levels as low as $W = 10$, collective bending and torsional motions can be neglected for short DNAs. In addition, uniform end-to-end tumbling can be neglected, because this type of motion is restricted in the solid state, even with a sample of intermediate hydration ($10 < W < 20$). Previous work has shown that uniform rotation of the DNA around the helix axis occurs at $W = 10$ and above and is effectively simulated by a six-site jump,[41] with a half angle of $\Theta = 20°$ (orientation of the local dynamic axis of the C2′–^{2}H2″ bond with respect to the longitudinal helix axis); values of $\phi = 0°, 60°, 120°, 180°, 240°$, and 300° for the six sites; and a rate constant of $k \approx 1.0 \times 10^4$ Hz. Use of these parameters for the overall helixmotion has produced good agreement in previous work for several different DNA samples with different types of local motions occurring. These parameters are generally considered well-determined and remain constant for the simulations of the local motions. The resulting simulated spectra are superpositions of the uniform helical rotation and the local motion of the furanose ring.

Models of Furanose Ring Motion

To simulate the deuterium lineshapes for 2″ deuterons, a modeling framework previously successful in simulating furanose lineshapes has been utilized. The cyclic nature of the furanose ring reduces the number of independent geometrical parameters required to describe the displacement of the C–^{2}H bond. The basic structural features arise from the Herzyk and Rabczenko model,[42] in which the Cartesian coordinates of the jth heavy atom in the furanose ring are

$$\begin{aligned} x_j &= r_j \left[\sin\alpha_j \times \sin 2\left(\phi + \frac{4\pi j}{5}\right) - \cos\alpha_j \times \cos 2\left(\phi + \frac{4\pi j}{5}\right) + R_j \cos\alpha_j \right] y_i \\ &= -r_j \left[\cos\alpha_j \times \sin 2\left(\phi + \frac{4\pi j}{5}\right) - \sin\alpha_j \times \cos 2\left(\phi + \frac{4\pi j}{5}\right) + R_j \sin\alpha_j \right] z_j \\ &= \left(\frac{2}{5}\right)^{1/2} q \cos\left(\phi + \frac{4\pi j}{5}\right) \end{aligned} \tag{13}$$

where, α_j is the polar angle locating the *j*th bond, r_j is the radius of the projection of the atomic pseudorotation trajectory onto the plane of the undistorted ring, R_j is the distance from the geometric center of the planar five-membered ring to the center of the projection of the *j*th trajectory onto the plane of the undistorted furanose ring, *q* is the puckering amplitude (in Å), and ϕ is the pseudorotation phase. Given the structural constraints of a furanose ring, the only adjustable parameter is the pucker amplitude, *q*.

Equation 13 describes the coordinates of the heavy atom framework of the furanose ring as a function of ϕ. The model can be generalized to include the reorientation of the C–^{2}H bond.[23,24,34] For each value of pseudorotation phase angle ϕ, there corresponds a set of angles (Θ_{PC}, ϕ_{PC}) specifying the orientation of a C2′–^{2}H2″ bond relative to a coordinate system fixed to the framework of the planar furanose ring. The set of angles (Θ_{PC}, ϕ_{PC}) are then used to calculate the site frequencies $\omega_{\pm}^{i}$ according to eq 3.

The trajectory of the ^{2}H2″ deuteron corresponding to this set of angles is a slightly curved ellipse,[23,24,34] and the angular dispersion increases with puckering amplitude *q*. If the value of *q* is 0.4 Å, the total excursion along the direction of the major axis of the ellipse is 52° and the total excursion along the direction of the minor axis is about 20° degrees, whereas for *q* = 0.2 Å, the corresponding excursions along the major and minor semiaxes are about 28° and 10°, respectively.

To calculate the deuterium line shape with eqs 4–7, information is needed regarding the atomic trajectory as well as a form for the operator π in eq 2. Jumps between discrete sites is a good approximation when barriers separating the sites approach $10k_BT$, corresponding to a barrier of about 25 kJ/mol at T = 300 K. Instead of treating the motion of the C–^{2}H bond as a jump between discrete sites, the C2′–^{2}H2″ bond can be envisioned as diffusing over these low energy barriers. π then has the form of a steady state Fokker–Planck operator,

$$\pi = D\left[\frac{\partial^2}{\partial\phi^2} + \frac{1}{k_B T}U'(\phi)\frac{\partial}{\partial\phi} + \frac{1}{k_B T}U''(\phi)\right] \tag{14}$$

where $U(\phi)$ is the external potential in which the C–^{2}H bond diffuses and *D* is the orientation-independent diffusion coefficient associated with the motion of the C–^{2}H bond.

Solving eq 1 using the form for π given in eq 14 is difficult even for relatively simple forms for $U(\phi)$. Nadler and Schulten[43] have introduced a finite difference approximation for eq 14, where π is represented by a tridiagonal matrix with elements defined by

$$\begin{aligned} &\pi_{ij} = \frac{1}{\tau}\left(\frac{W_i}{W_{i\pm1}}\right)^{1/2}; \quad j = i \pm i \\ &\pi_{ij} = -\left(\pi_{i,j-1} + \pi_{i,j+1}\right); \quad j = 1 \\ &\pi_j = 0, \text{ otherwise} \end{aligned} \tag{15}$$

where in eq 15 $W_i = e^{-U(\phi_i)/k_BT}/Q$ and Q is the partition function. The diffusion coefficient, D, can be expressed in terms of the correlation time (τ_c) as well as the kinetic rate constant (k) and the unit angular step (δ) where $1/2\tau_c = D = k\delta^2/2$. This formulation has been used to describe the motion of heme groups in proteins,[44] amino acid side chains in proteins,[45] and polymethylene chains in lipids.[46] The continuous trajectory is therefore discretized into a small (ca. 10) number of individual steps, which are then incorporated into the MXET1 rate matrix. The rate constant k and the associated diffusion coefficient D represent transitions between individual sites along this discretized trajectory. Each site then has associated angular components owing to the 3D orientations of a C–^{2}H bonds going through pseudorotation and site populations according to eq 15.

To simulate the motion of the furanose ring, a form of the potential $U(\phi)$ must be chosen. Initial studies modeling highly dynamic furanose rings from ^{2}H SSNMR used a two-site jump model,[30,32] in which the implicit assumption is that the two sites represent the bottom of potential energy wells corresponding to two primary pseudorotation conformers and that there is a large ($\geq$10 k_BT) barrier between the wells. Other models[34] built upon this work to use a two-well potential energy surface[47-49] with barriers on the order of 5 k_BT. Further development of different potentials includes unequal double-well, weighted double-well, single-well, and harmonic energy surfaces.[23,24] All of these potentials can be approximated with simple analytical equations, making them good candidates for use in this analysis. Their equations and graphical representations are given in Table 1 and Figure 2.

The lowest energy region for each type of surface, represented by the bottom of each well, was assumed to be a value of $\phi = 180°$, which corresponds very closely to the C2′-endo pseudorotation conformation. This was considered to be our lowest energy conformation, because it is the primary furanose ring conformation observed in high-resolution structures of DNA.

To determine the best fit equilibrium line shapes, a library of hundreds of simulated spectra are generated varying the puckering amplitude q (eq 13), the rate constant k between sites along the pseudorotation trajectory (eq 14), the form of the potential $U(\phi)$, and the “barrier height” U_0 (both from Table 1), offering a small number of independent variables in the analysis.

IV. Results

Unsymmetrized quadrupole echo lineshapes for DNAs containing T:A and U:A base pairs are given in Figure 3. Visual inspection of the lineshapes indicates they are essentially identical within the limits of the noise level. The T:A line shape has some modest differences when compared to initial studies on an identical DNA sequence,[31] but these could be attributed to T_{2e} effects due to the difference in field strength or perhaps small differences in hydration or sample conditions.

Figure 4 shows the raw data and fits for the $\langle T_{2e} \rangle$ relaxation experiments obtained for both the T:A and U:A samples. $\langle T_{2e} \rangle$ relaxation times are listed, along with standard deviations, in Table 2. Spectra are shown as a function of the delay time, τ, between the two pulses of the quadrupolar echo. Because relaxation occurs during both τ periods, T_2 is twice the time constant of the exponential. The values for these relaxation times are nearly equal within experimental error and are likely dominated by dipolar coupling of the deuterons to the other proton on the methylene group. Using a model that assumes a single proton at 1.8 Å, rotating with a ^{1}H- ^{2}H vector at 15° to the helix axis (as would be predicted by the canonical B-DNA structure) an exponential fit to the distinctly nonexponential time evolution of the echo down to the point that the echo is at 10% of its original intensity yields a crude estimate of $T_{2,dipolar}$ of 180 μs. Allowing for lesser but still significant contributions from more distant protons, it appears that

transverse relaxation is dominated by the heteronuclear dipolar interaction, and the contribution from slow motional modulation of the quadrupolar interaction is small.

Figure 5 shows the raw data and fits for the saturation recovery experiments to obtain $\langle T_1 \rangle$ for both the T:A and U:A samples. In this case, the experimental spin–echoes are shown as a function of the relaxation delay t_D between successive acquisitions. Powder-averaged spin–lattice relaxation times, obtained by a two-parameter fit to the function $I = I_\infty[1 - \exp(t_D/T_1)]$ are listed in Table 2. The values for these relaxation times suggest that the faster motions within the two samples are also nearly indistinguishable. The relaxation results coupled with the essentially identical quadrupolar echo line shapes suggest that the two samples have indistinguishable dynamic properties.

The simulated spectrum that provides the best fit to the symmetrized experimental results is shown in Figure 6. It was generated by superpositions of the uniform helical rotation and the local motion of the furanose ring. The local motion was simulated as described above. The best fit simulation arises by using a Hookean/harmonic potential for the potential energy surface (Figure 2e), with a value of U_0 of 5.5 k_BT. The rate constant between sites along the pseudorotation trajectory is 1.0×10^7 Hz, which leads to a value of 2.0×10^6 rad^2/s for the diffusion constant, D. The puckering amplitude is $q = 0.5$ Å. Additionally, there is a structural difference between this simulation and those performed previously. The angle of the C–^{2}H bond relative to the longitudinal helix axis was determined to be $\Theta = 25°$.

It can be shown that the local motions present contribute significantly to the overall line shape. Figure 7 builds up the motions one at a time. First, in Figure 7a is a static line shape. Figure 7b contains only the helical motions present due to the filled first hydration shell. Figure 7c shows a small amplitude (10°) local libration of the C–^{2}H bond, and Figure 7d repeats the best fit simulation, confirming that there is contribution from nonactivated motion.

V. Discussion

The results from this work lead to the conclusion that there is essentially no difference in the dynamics of the furanose rings for DNA containing uracil compared to a thymine in the same sequence context. This conclusion was drawn from the lack of discernible differences in quadrupole echo lineshapes, $\langle T_1 \rangle$ and $\langle T_{2e} \rangle$ values. These results are analogous, but less dramatic than those seen in the M. *Hha*I binding sequence.[23] The *Hha*I methyltransferase uses a nucleotide flipping mechanism during its conversion of cytosine to 5-methylcytosine,[26] similar to UNG. Deuterium SSNMR indicates a significant difference in motions between the target deoxycytidine residue and the surrounding sequence.[23] However, the differences in the equilibrium line shapes and simulated line shape parameters between the deoxycytidine substrate sequence and the methylated analogue are more subtle. It was concluded that the unmethylated site has a modestly larger puckering amplitude (0.40 Å for C versus 0.35 Å for 5-methyl-C).[23] This indicates that although there is a significant sequence dependence on local dynamic properties, there may be a smaller dependence upon modifications of the target DNA base. The results herein for furanose ring line shapes and relaxation times are analogous in that they compare samples that contain uracil versus thymine which, like cytosine and 5-methyl-cytosine, differ only by the presence of a single methyl group. Given the identical base pairing and the small steric difference between the two bases, it is perhaps not surprising that demethylation of the DNA leads to no detectable dynamic perturbation.

It must be stated that the lack of distinct spectral features suggests a difficulty in providing nondegenerate simulations that fit the experimental line shapes. The results from the simulations presented do offer some insight into the local motions, as well. Although the harmonic potential is without a significant energy “barrier” to conformational rearrangement,

it can be seen in Figure 2 that the angular dependence to the barrier is significant, and the pseudorotational conformations outside the bottom of the well will not be highly populated. Indeed, this is indicated in Figure 8, which displays populations of sites within the trajectory used in the best fit simulation and compares them to the site populations of an unequal two-well potential (Figure 2b) with barrier heights $5k_BT$ and $1k_BT$. These data suggest that these sugar rings, undergoing motion within this harmonic well, are only sampling a small number of conformations. This result is consistent with previous data for the T:A indicating small angle motion,[31] that even though the overall angular excursion of the sugar ring is large (0.5 Å), only a small number of these sites are highly populated.

What is the importance, if any, of these similar motions and what conclusions can be drawn from this work? Taken initially, these results may seem to contradict the hypothesis of a dynamic component to lesion recognition, and this is certainly a possible interpretation. In particular, the replacement of thymine with uracil while base pairing with adenine represents one of the least significant structural alterations, and this type of structural disruption may provide relatively small effects on the overall DNA properties. Sequences containing other lesions are currently being examined.

The differences between the U:A and T:A samples are indistinguishable, indicating that a purely dynamic recognition process via local motions of the furanose ring is unlikely to be the sole arbiter of specificity. Indeed, other aspects, including steric hindrance and electronic properties of the 5-substituent and thermal stability of base pairing partners, have been proposed as other means of discrimination.[50] The current work agrees well with established data on several fronts. First, uracil base-paired with adenine provides lower activity in uracil DNA glycosylases from various organisms[50-53] as well as other DNA glycosylases with uracil as a substrate,[15] relative to U:G base pairs. Additionally, U:A base pairs have significantly different melting thermodynamic properties relative to U:G base pairs (as well as other base-pairing contexts).[15] If there is a dynamic component to recognition, they may be exhibited more strongly in a U:G base pair than in a U:A base pair.

Sequence context may also play an important factor. It has been stated that for uracil recognition, sequence plays a greater role than base pairing in determining repair enzyme activity.[51-53] When a large number of sequences were tested for activity, the flanking sequence for the samples in this work (i.e., 5′-AATUCG-3′) offered a relatively low activity compared to the optimum flanking sequence (5′-GCAUAA-3′).[51,52] Flexibility in the nearest neighbors of a uracil has also been proposed as an aspect of recognition from fluorescence studies.[54] Sequence dependence may ultimately result from differences in base stacking energies between the uracil and its neighbors. Differences in base stacking have been suggested as playing a role in recognition of thymine in T:G base pairs.[15,54]

If there is a dynamic component of discrimination or recognition, there may be other reasons that differences do not appear in these two samples. First, the important subunits responsible may be other than the furanose ring. In fact, the backbone methylene group in C:G base pairs has significantly different local motions than in 5-Me-C:G base pairs.[24] The backbone moiety contains dihedral angles that must be altered significantly during the nucleotide flipping process, and it may be these that have significantly lowered energy barriers in lesion-containing DNAs. Second, the time scale of motions may be beyond the region accessible by the experiments performed, and it has been proposed that U:G removal happens faster than U:A removal.[52]

VI. Conclusion

This paper offers insight into the local dynamic properties of DNA containing the single-base lesion uracil base-paired to adenine. To our knowledge, this work represents the first site-specific ^{2}H SSNMR study of damaged DNA dynamics. Given the importance of understanding the functional roles of dynamics in biomolecular recognition, analysis and quantification of these motions becomes important in determining their role. Our results suggest the presence of a uracil base pairing with adenine does not alter the dynamics of the furanose ring from line shape and relaxation analysis. Therefore, a dynamic component of uracil recognition via the furanose ring is unlikely to be the sole arbiter of specificity for uracil DNA glycosylase.

Acknowledgments

This research was funded by grants from the National Institutes of Health (R01 GM 065252) and DARPA/SPAWAR (N66001-08-1-2026) to G.S.H., by a grant from the National Institutes of Health (R15 CA130008-01A1) and by an award from Research Corporation to GAM, and by funds from the University of Missouri–Kansas City College of Arts and Sciences to N.A.O. We thank Dr. R. Stephen Lloyd for his thoughtful commentary and suggestions and Dr. Joe Dumais for assistance on the data acquisition.

References and Notes

(1). Schärer OD. Angew. Chem., Int. Ed 2003;42:2946.

(2). Sousa MML, Krokan HE, Slupphaug G. Mol. Aspects Med 2007;28:276. [PubMed: 17590428]

(3). Krokan HE, Standal R, Slupphaug G. Biochem. J 1997;325:1. [PubMed: 9224623]

(4). McCullough AK, Dodson ML, Lloyd RS. Annu. Rev. Biochem 1999;68:255. [PubMed: 10872450]

(5). Stivers JT, Jiang YL. Chem. Rev 2003;103:2729. [PubMed: 12848584]

(6). Fromme JC, Verdine GL. Adv. Protein Chem 2004;69:1. [PubMed: 15588838]

(7). Huffman JL, Sundheim O, Tainer JA. Mut. Res 2005;577:55. [PubMed: 15941573]

(8). Zharkov DO, Grollman AP. Mut. Res 2005;577:24. [PubMed: 15939442]

(9). Roberts RJ, Cheng X. Annu. Rev. Biochem 1998;67:181. [PubMed: 9759487]

(10). Slupphaug G, Mol CD, Kavli B, Arvai AS, Krokan HE, Tainer JA. Nature 1996;384:87. [PubMed: 8900285]

(11). Lukin M, de los Santos C. Chem. Rev 2006;106:607. [PubMed: 16464019]

(12). Delort A-M, Neumann JM, Molko D, HervéTéoule R, Dinh S. Tran. Nucleic Acids Res 1985;13:3343. [PubMed: 4000973]

(13). Ghosh M, Kumar NV, Varshney U, Chary KVR. Nucleic Acids Res 2000;28:1906. [PubMed: 10756190]

(14). Dong J, Drohat AC, Stivers JT, Pankiewicz KW, Carey PR. Biochemistry 2000;39:13241. [PubMed: 11052677]

(15). Liu P, Theruvathu JA, Darwanto A, Lao VV, Pascal T, Goddard W III, Sowers LC. J. Biol. Chem 2008;283:8829. [PubMed: 18208817]

(16). Stivers JT. Prog. Nucleic Acid Res. Mol. Biol 2004;77:37. [PubMed: 15196890]

(17). Yang W. Cell Res 2008;18:184. [PubMed: 18157156]

(18). Cao C, Jiang YL, Stivers JT, Song F. Nat. Struct. Mol. Biol 2004;11:1230. [PubMed: 15558051]

(19). Parker JB, Bianchet MA, Krosky DJ, Friedman JI, Amzel LM, Stivers JT. Nature 2007;449:433. [PubMed: 17704764]

(20). Sundina AE, Volkov EM, Kubareva EA. Biocatalysis 2000;41:121.

(21). Meints G, Drobny G. Biochemistry 2001;40:12436. [PubMed: 11591165]

(22). Miller PA, Shajani Z, Meints GA, Caplow D, Goobes G, Varani G, Drobny GP. J. Am. Chem. Soc 2006;128:15970. [PubMed: 17165714]

(23). Meints GA, Miller PA, Pederson K, Shajani Z, Drobny GP. J. Am. Chem. Soc 2008;130:7305. [PubMed: 18489097]

(24). Pederson K, Meints GA, Shajani Z, Miller PA, Drobny GP. J. Am. Chem. Soc 2008;130:9072. [PubMed: 18570423]

(25). Echodu D, Goobes G, Shajani Z, Pederson K, Meints GA, Varani G, Drobny GP. J. Phys. Chem. B 2008;112:13934. [PubMed: 18844399]

(26). Klimasauskas S, Kumar S, Roberts RJ, Cheng X. Cell 1994;76:357. [PubMed: 8293469]

(27). Robins MJ, Wilson JS, Hansske FJ. Am. Chem. Soc 1983;105:4059.

(28). Gait, MJ., editor. Oligonucleotide Synthesis: A Practical Approach. IRL Press; Oxford: 1984. Practical Approach Series

(29). Dickerson RE, Drew HR. J. Mol. Biol 1981;149:761. [PubMed: 6273591]

(30). Huang W-C, Orban J, Kintanar A, Reid BR, Drobny GP. J. Am. Chem. Soc 1990;112:9059.

(31). Hatcher, ME. Ph.D. Thesis. University of Washington; Seattle, WA: 1996. A Solid-State Deuterium NMR Investigation of the Local Dynamics of Nucleotides in the EcoRI Restriction Endonuclease Binding Site.

(32). Hatcher ME, Mattielo DL, Meints GA, Orban J, Drobny GP. J. Am. Chem. Soc 1998;120:9850.

(33). Geahigan KB, Meints GA, Hatcher ME, Orban J, Drobny GP. Biochemistry 2000;39:4939. [PubMed: 10769153]

(34). Meints GA, Karlsson T, Drobny GP. J. Am. Chem. Soc 2001;123:10030. [PubMed: 11592881]

(35). Lide, DR. Handbook of Chemistry and Physics. Vol. Vol. 84. CRC Press; Boca Raton, Fla.: 2003-2004. p. 15-26.

(36). Falk M, Hartman KA, Lord RC. J. Am. Chem. Soc 1962;84:3843.

(37). Wang AC, Kennedy MA, Reid BR, Drobny GP. J. Magn. Reson 1994;105:1.

(38). Schurr JM, Fujimoto BS, Diaz R, Robinson BH. J. Magn. Reson 1999;140:404. [PubMed: 10497047]

(39). Torchia S, Szabo AJ. Magn. Reson 1982;49:107.

(40). Vold, RR.; Vold, RL. Advances in Magnetic and Optical Resonance. Warren, W., editor. Vol. Vol. 16. Academic Press; San Diego: 1991. p. 85-171.

(41). Alam T, Drobny GP. Chem. Rev 1991;91:1545.

(42). Herzyk P, Rabczenko A. J. Chem. Soc. Perkin Trans. II 1985:1925.

(43). Nadler W, Schulten KJ. Chem. Phys 1986;84:4015.

(44). Nadler W, Schulten L. Proc. Natl. Acad. Sci. U.S.A 1984;81:5719. [PubMed: 6592583]

(45). Wittebort R, Szabo A. J. Chem. Phys 1978;69:1722.

(46). Wittebort RJ, Olejniczak ET, Griffin RG. J. Chem. Phys 1987;86:5411.

(47). Levitt M, Warshel A. J. Am. Chem. Soc 1978;100:2607.

(48). Olson WK. J. Am. Chem. Soc 1982;104:278.

(49). Saenger, W. Principles of Nucleic Acid Structure. Springer Verlag; New York: 1984.

(50). Liu P, Burdzy A, Sowers LC. Chem. Res. Toxicol 2002;15:1001. [PubMed: 12184783]

(51). Nilsen H, Yazdankhah SP, Eftedeal I, Krokan HE. FEBS Lett 1995;362:205. [PubMed: 7720873]

(52). Slupphaug G, Eftedal I, Kavli B, Bharati S, Helle NM, Haug T, Levine DW, Krokan HE. Biochemistry 1995;34:128. [PubMed: 7819187]

(53). Bellamy SRW, Baldwin GS. Nucleic Acids Res 2001;29:3857. [PubMed: 11557818]

(54). Allawi HT, SantaLucia J Jr. Biochemistry 1997;36:10581. [PubMed: 9265640]

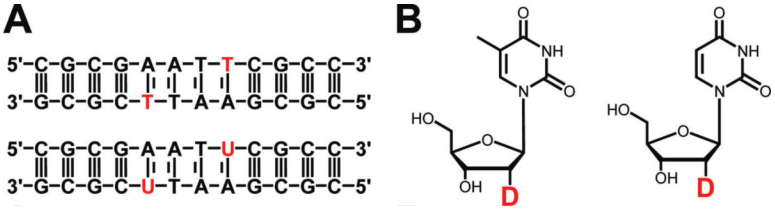

Figure 1.

(A) Palindromic DNA sequences used in this study. The red indicates the residues containing the [2″-^{2}H] label. (B) Location of the deuterium label on the thymidine (left) and deoxyuridine (right) residues indicated in red in part A.

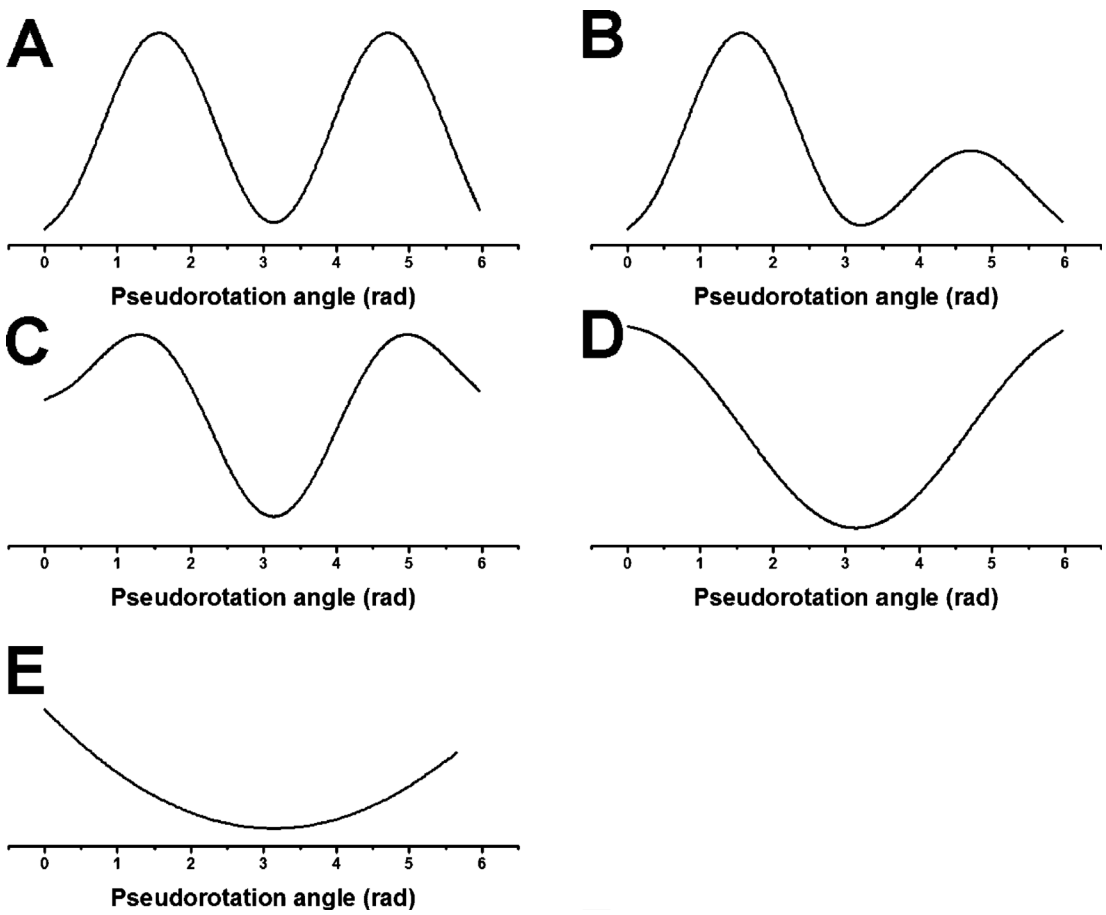

Figure 2.
Angular dependent potential energies used in simulations described in text: (A) equal double well, (B) unequal double well, (C) weighted double well, (D) single well, and (E) harmonic.

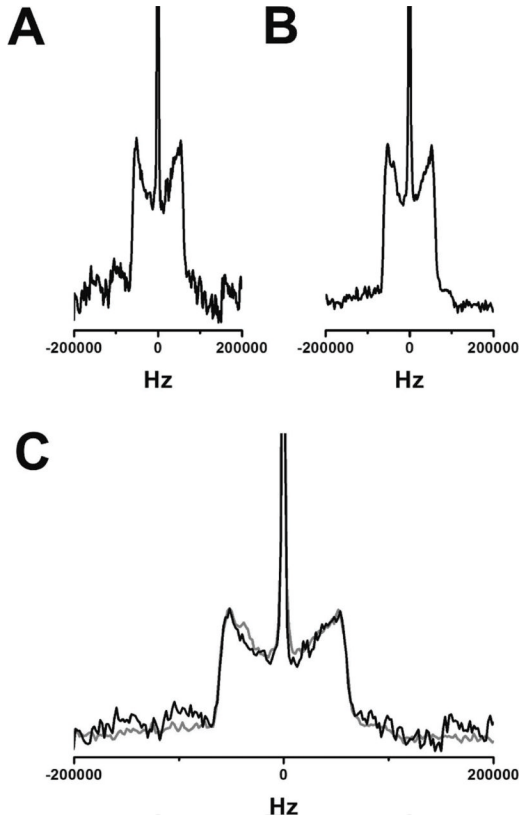

Figure 3.
Comparison of quadrupole echo lineshapes for (A) T:A and (B) U:A samples and (C) overlaid where the T:A sample is in black and the U:A sample in red. Note that central isotropic peaks are residual HDO.

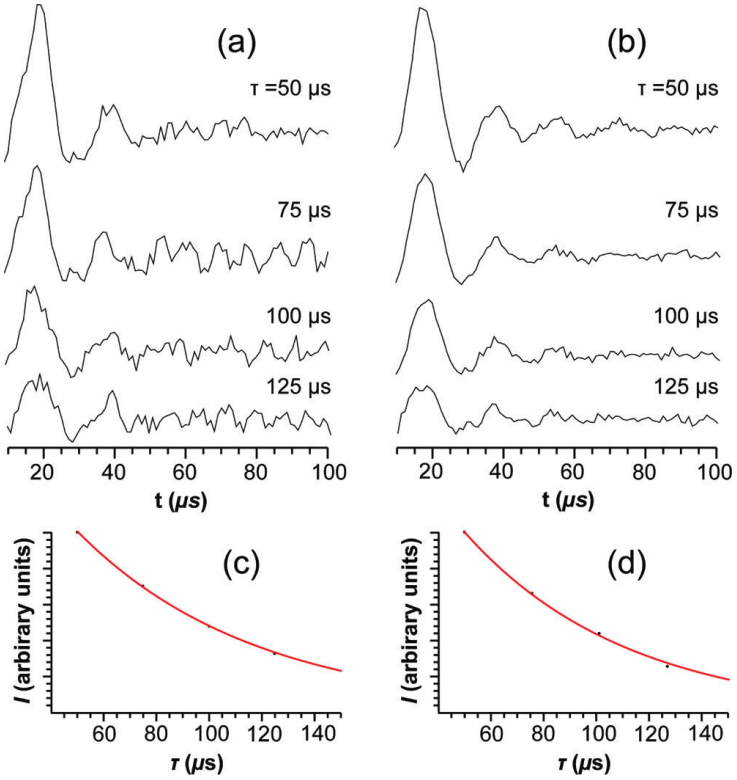

Figure 4.

$\langle T_{2e} \rangle$ data and fits. (a) Spin echoes for T:A, as a function of the time τ between the two $\pi/2$ pulses. (b) Spin echoes for U:A, as a function of the time τ between the two $\pi/2$ pulses. (c) Exponential fit to echo intensities as a function of τ for the T:A sample. (d) Exponential fit to echo intensities as a function of τ for the U:A sample.

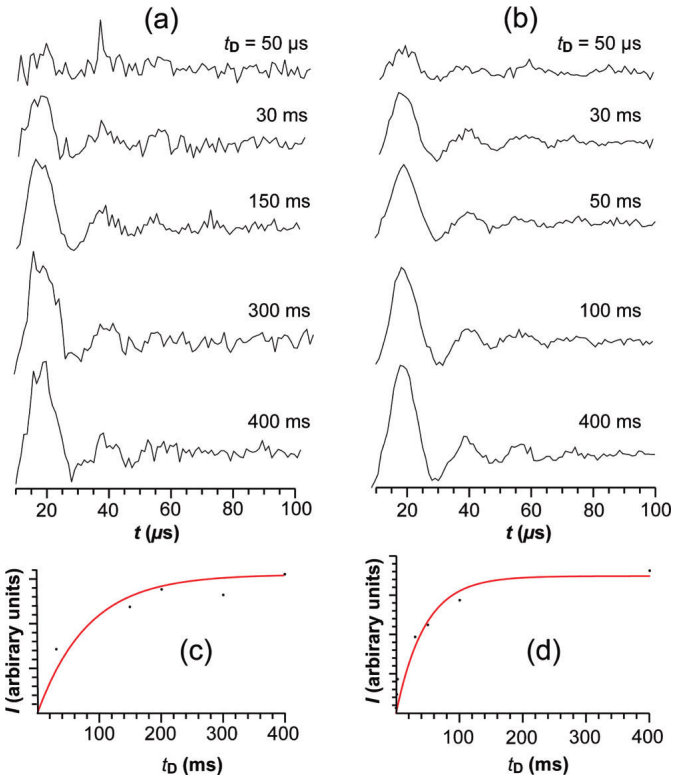

Figure 5.

$\langle T_1 \rangle$ data and fits. (a) Spin echoes for T:A, as a function of the relaxation delay t_D. (b) Spin echoes for U:A, as a function of the relaxation delay t_D. (c) Exponential fit to echo intensities as a function of t_D for the T:A sample. (d) Exponential fit to echo intensities as a function of t_D for the U:A sample.

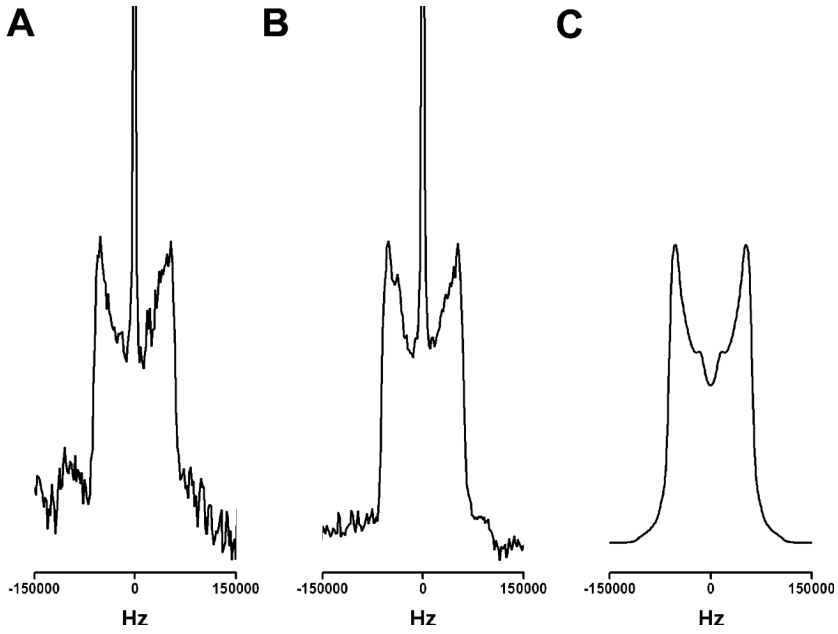

Figure 6.

Comparison of the T:A (A) and U:A (B) experimental lineshapes to the best fit simulation (C). The specific simulation parameters are discussed in the text. Note that central isotropic peaks are residual HDO.

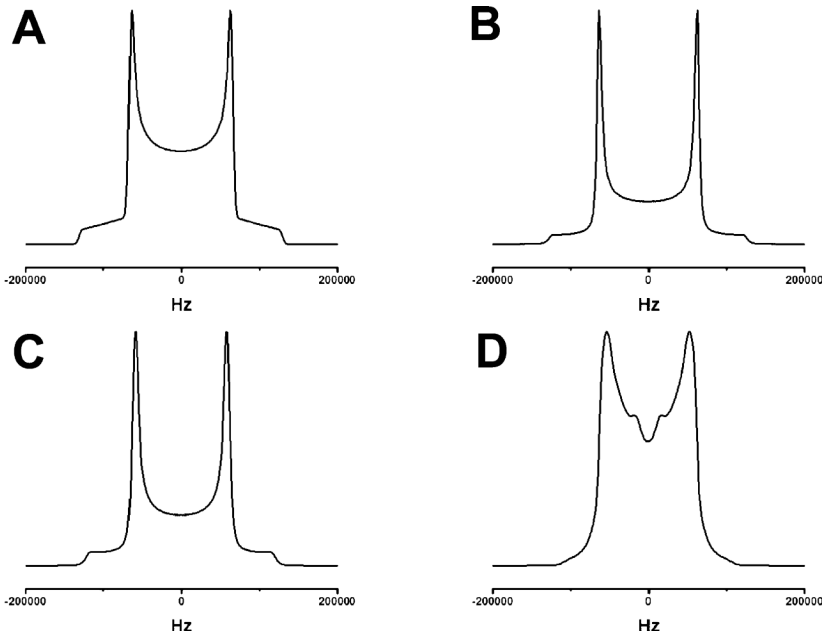

Figure 7.

Simulation build-up for the best fit to the experimental data. (A) Static deuterium line shape. (B) Line shape containing only six-site slow helical rotation. (C) Line shape with small angle (10°) libration for local motion of the sugar ring superimposed on the slow helical motion. (D) Best fit simulation with specific details discussed in the main text.

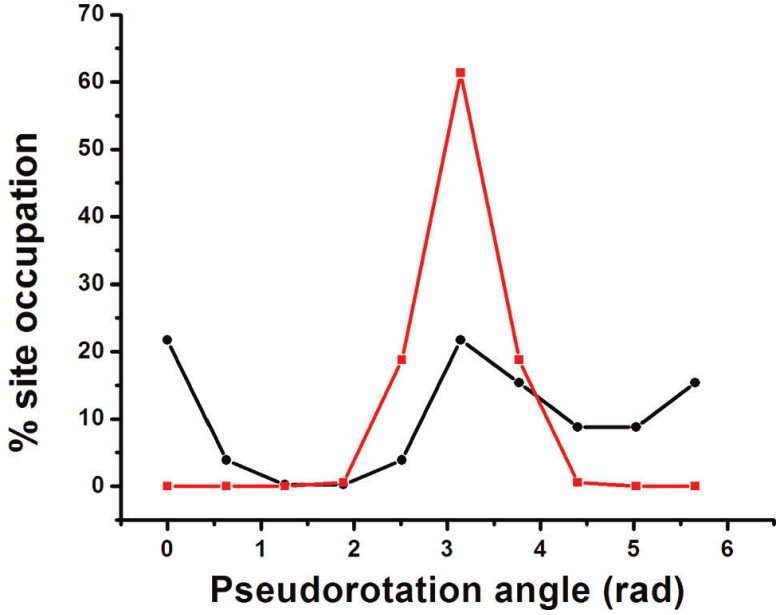

Figure 8.

Overlay of the site populations for the trajectories of the potential energy used in the best fit simulations (red) for U:A and T:A compared to an arbitrary unequal double (Figure 2b) well of barrier heights $5k_BT$ and $1k_BT$ (black). The symbols represent the 10 sites along the discretized trajectory.

TABLE 1

Analytical Expressions of the $U(\phi)$ Angular Dependent Potential Energies Used for Simulation Library

type of surface	analytical expression
equal double well	$U\left(\phi\right) = \frac{U_0}{2}\left(1 - \cos 2\phi\right)$
unequal double well	$U\left(\phi\right) = \frac{U_{0_1}}{2}\left(1 - \cos 2\phi\right),\ 0 < \phi < \pi$
	$U\left(\phi\right) = \frac{U_{0_2}}{2}\left(1 - \cos 2\phi\right),\ \pi < \phi < 2\pi$
weighted double well	$U\left(\phi\right) = \frac{U_{0_1}}{2}\left(1 - \cos 2\phi\right),\ \frac{\pi}{2} < \phi < \frac{3\pi}{2}$
	$U\left(\phi\right) = \frac{U_{0_1}}{2}\left(W\left(1 - \cos 2\phi\right)\right),\ \frac{3\pi}{2} < \phi < \frac{\pi}{2}$
single well	$U\left(\phi\right) = \frac{U_0}{2}\left(1 - \cos \phi\right)$
harmonic	$U\left(\phi\right) = \frac{\kappa}{2}\left(\phi - \phi_0\right)^2$

TABLE 2

Comparison of Relaxation Times between T:A and U:A Samples

relaxation time	T:A sample	U:A sample
$\langle T_{2e} \rangle$	134.6 (± 2.0) μs	120.4 (± 4.4) μs
$\langle T_1 \rangle$	52.6 (± 12.8) ms	45.3 (± 15.4) ms